



Computational and structural evidence for neurotransmitter-mediated modulation of the oligomeric states of human insulin in storage granules

Received for publication, January 9, 2017, and in revised form, March 23, 2017. Published, Papers in Press, March 27, 2017, DOI 10.1074/jbc.M117.775924

Vladimír Palivec[‡], Cristina M. Viola[§], Mateusz Kozak^{§1}, Timothy R. Ganderton[§], Květoslava Křížková[‡], Johan P. Turkenburg[§], Petra Halušková[‡], Lenka Žáková[‡], Jiří Jiráček^{‡2}, Pavel Jungwirth^{‡3}, and Andrzej M. Brzozowski^{§4}

From the [§]York Structural Biology Laboratory, Department of Chemistry, University of York, Heslington, York YO10 5DD, United Kingdom and [‡]Institute of Organic Chemistry and Biochemistry, Academy of Sciences of the Czech Republic, v.v.i., Flemingovo nám 2, 166 10 Prague 6, Czech Republic

Edited by Jeffrey E. Pessin

Human insulin is a pivotal protein hormone controlling metabolism, growth, and aging and whose malfunctioning underlies diabetes, some cancers, and neurodegeneration. Despite its central position in human physiology, the *in vivo* oligomeric state and conformation of insulin in its storage granules in the pancreas are not known. In contrast, many *in vitro* structures of hexamers of this hormone are available and fall into three conformational states: T₆, T₃R₃^f, and R₆. As there is strong evidence for accumulation of neurotransmitters, such as serotonin and dopamine, in insulin storage granules in pancreatic β -cells, we probed by molecular dynamics (MD) and protein crystallography (PC) if these endogenous ligands affect and stabilize insulin oligomers. Parallel studies independently converged on the observation that serotonin binds well within the insulin hexamer (site I), stabilizing it in the T₃R₃ conformation. Both methods indicated serotonin binding on the hexamer surface (site III) as well. MD, but not PC, indicated that dopamine was also a good site III ligand. Some of the PC studies also included arginine, which may be abundant in insulin granules upon processing of pro-insulin, and stable T₃R₃ hexamers loaded with both serotonin and arginine were obtained. The MD and PC results were supported further by in solution spectroscopic studies with R-state-specific chromophore. Our results indicate that the T₃R₃ oligomer is a plausible insulin pancreatic storage form, resulting from its complex interplay with neurotransmitters, and pro-insulin processing products.

These findings may have implications for clinical insulin formulations.

Insulin is one of the key human protein hormones that is responsible for the maintenance of metabolic homeostasis, with an influence on cell proliferation and regulation of aging (1, 2). Defects in insulin bioavailability or impaired insulin receptor signaling lead to different pathological conditions such as diabetes (3–5), cancers (6–8), and Alzheimer's disease (9).

Insulin is a 51-amino acid protein consisting of two disulfide-linked chains (A1–A21, B1–B30) and exerts its functions through binding as a monomer to the ($\alpha\beta$)₂ heterodimer tyrosine-kinase-type insulin receptor (IR)⁵ (10, 11). Insulin is produced from a single chain pro-insulin and stored in pancreatic β -cells in storage granules (termed large dense core vesicles (LDCVs)) from which it is released into the bloodstream in response to elevated blood glucose levels. The first 3D crystal structure of insulin was described by Hodgkin and coworkers in 1969 (12) in the form of its hexameric assembly (with three and two-fold rotational symmetry (*i.e.* trimer of dimers), obtained in the presence of Zn²⁺ ions. Two Zn²⁺ ions were identified in the hexamer on its 3-fold axis, being coordinated by 3 imidazole side chains of His^{B10}. This and subsequent similar findings resulted in a generally accepted paradigm that the hexamer is the storage form of insulin in LDCVs in pancreatic β -cells, whereas upon its release into the bloodstream it dissociates to monomers, which represent the active form of the enzyme (13). The pioneering work of D. C. Hodgkin was followed by 3D descriptions of hundreds of *in vitro* studied insulin hexamers, dimers, and monomers (for reviews, see for example Refs. 14–16). However, the actual *in vivo* storage form of insulin in pancreatic β -cells LDCVs is still not known, and it is extrapolated from its *in vitro* structures. Surprisingly, there are more advances into the very elusive nature of insulin/IR interactions (17, 18) than into the *in vivo* form of this hormone, investigation of which presents formidable experimental challenges.

This work was also supported by the Research Project of the Czech Academy of Sciences RVO:61388963 (to the Institute of Organic Chemistry and Biochemistry). This work was also supported by Medical Research Council Grant MR/K000179/1 (to A. M. B.), and Supported by Czech Science Foundation Grant 16–010745 (to P. J.). The authors declare that they have no conflicts of interest with the contents of this article.

✂ Author's Choice—Final version free via Creative Commons CC-BY license. The atomic coordinates and structure factors (codes 5MAM, 5MT3, and 5MT9) have been deposited in the Protein Data Bank (<http://www.pdb.org/>).

This article contains supplemental Tables S1–S4 and Figs. S1–S7.

¹ Present address: Dept. of Biochemistry, University of Geneva, Quai Ernest-Ansermet 30, 1205 Geneva, Switzerland.

² To whom correspondence may be addressed. Tel.: 420-220-183-441; E-mail: jiracek@uochb.cas.cz.

³ To whom correspondence may be addressed. Tel.: 420-220-410-314; E-mail: pavel.jungwirth@uochb.cas.cz.

⁴ To whom correspondence may be addressed. Tel.: 44-1904-328265; Fax: 44-1904-328266; E-mail: marek.brzozowski@york.ac.uk.

⁵ The abbreviations used are: IR, insulin receptor; LDCV, large dense core vesicle; 4H3N, 4-hydroxy-3-nitrobenzoic acid; InsPheR₆, insulin R₆-state hexamer; r.m.s.d., root mean square deviation; HB, hydrogen-bonded.

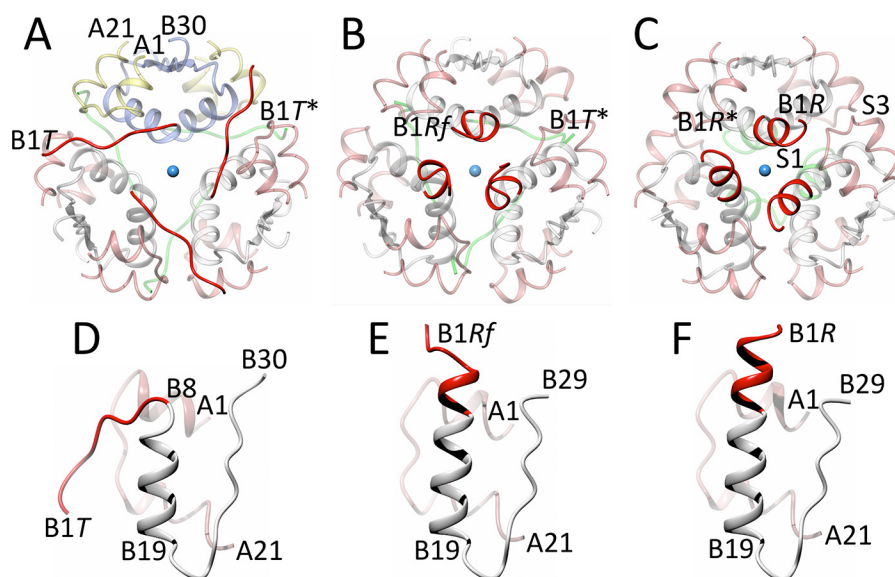


Figure 1. General structural organization of the three main forms of insulin hexamer: T_6 (A), $T_3R_3^f$ (B), and R_6 (C) in the hexamer top view along its 3-fold symmetry axis. Insulin B chains are in white, A chains are in pink; the chains of one representative insulin dimer are indicated in A in light blue (B-chains) and yellow (A-chains). Some N and C termini of one dimer are also indicated in A and only B-chain N termini in B and C, with * corresponding to the symmetry-related monomer within a dimer. The B1-B8 segments of the B chains that contribute to the largest structural changes in TR transitions are in red (top of the hexamer) and in green (bottom of the hexamer). The Zn^{2+} ion is in blue. D–F, representative insulin monomers in T, R^f , and R-state, respectively, with a coloring code as in A–C. Typical, main ligand binding sites I and III in the R insulin form are indicated in C as S1 and S3 respectively.

The *in vitro* data showed that insulin hexamers can be grouped into three structurally distinct states/families: T_6 , $T_3R_3^f$, and R_6 (15, 16), which differ by the conformation of the B1–B6 N termini of the hormone B-chain (see Fig. 1 and supplemental Fig. S1). In the T_6 hexamers, the initial B1–B6 segments of the B chains are fully extended followed by B7–B10 type II' β -turns that go into invariant B9–B19 α -helices. In contrast, the B1–B6 segments acquire an α -helical conformation in the R-state, extending the B9–B19 α -helix (19). The insulin R_3^f state is similar to the α -helical R_6 state; however, the long R-state B-chain helix is shortened to the B3–B19 segment, whereas the B1–B3 residues depart (“fray”) from the α -helical fold (20, 21). The TR^f transition can be induced by an increase of, for example, the concentration of Zn^{2+} , SCN^- , and Cl^- ions (22) or by the presence of phenolic derivatives (e.g. phenol or similar small cyclic alcohols) at low concentrations (23–25). The R^fR (or full TR) transition can be accomplished by a further increase of the concentration of phenolic ligands (19, 24). The octahedral Zn^{2+} coordination is also a signature of the T-state (assured by three His^{B10} imidazoles and three water molecules), whereas the Zn^{2+} tetrahedral coordination (three His^{B10} and, for example, a Cl^- ion) is typical for the R^f/R -states (e.g. Ref. 26). This coordination switch results from a smaller space above the Zn^{2+} ion in the R-state that is obstructed there by a longer B1–B8 helical part of the B9–B19-helix and a newly formed binding pocket for cyclic alcohols on the dimer interface, formed by the side chains of A6–7, A9–11, A16, B7, B11, and B5–7 (the so-called site I, or phenol main-binding site). However, variations of the Zn^{2+} coordination spheres are also observed frequently (27).

Although site I is the main binding cavity for all phenol-like ligands, they have also been identified in other regions of the hexamers; e.g. site II, formed by side chains B9, B12, B16, B17, B9, B10, B13; site I/II formed by B10, B14, B16, B17, and B9 (28).

Hexamer surface-exposed (between insulin dimers) phenolic site III (A14, A17) has been observed as well (29). The serendipitous character of the discovery of the phenol-stabilized R-state resulted from the bactericide-like applications of phenol in clinical formulations of insulin. Nevertheless, the R-like states of the hormone have clinical importance, as the R^f/R -trimers/hexamers are more stable (30). This is mostly due to the slower Zn^{2+} -solvent exchange, which results in a higher hexamer-monomer dissociation constant. However, the physiological relevance of T/ R^f /R states for an effective insulin/IR binding and for the storage form of the hormone (e.g. protection against proteolysis) is still unknown.

Here, we attempt to shed light on a possible conformation of the *in vivo* storage form of insulin in insulin-containing granules in pancreatic β -cells. Although the exact chemical composition of LDCVs still awaits full characterization, they contain Zn^{2+} ions and phenolic neurotransmitters such as dopamine and serotonin, which are involved in regulation of exocytosis of the granules and insulin release (31–33). Therefore, we hypothesize that both neurotransmitters can bind to, and affect the structure of insulin hexamers, assembled in the presence of zinc cations. We probe these effects in parallel via molecular dynamics simulations (MD) and protein X-ray crystallography. These were further supplemented by spectroscopic studies with the use of a sensitive chromophore, 4-hydroxy-3-nitrobenzoic acid (4H3N), which specifically binds to R-state insulin as indicated by a red shift of its absorption spectrum. Moreover, as arginine can accumulate in LDCVs upon processing of pro-insulin at its two Arg-rich sites (34, 35) and as arginine-rich polypeptides (spermine/spermidine) are used in some insulin injections formulations (36, 37), we also probe the structural effect of this amino acid on insulin oligomeric assembly.

Both the MD and X-ray serotonin-related studies point to a stable insulin hexamer-serotonin-site I complex and its

Structural forms of storage insulin in pancreas

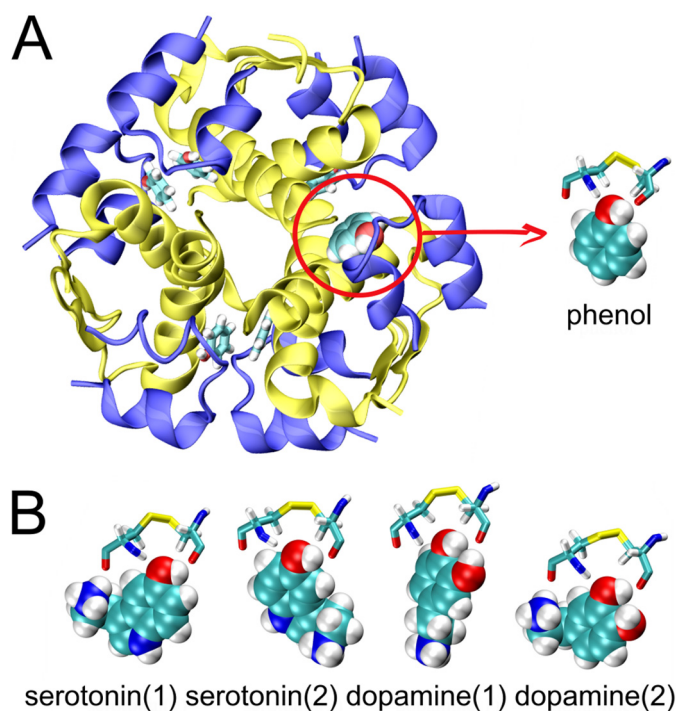


Figure 2. Starting conformations of phenol (A, insulin R₆ hexamer shown for the sake of clarity of the phenolic pocket location), serotonin (B), and dopamine (B) molecules (depicted by van der Waals spheres) in the phenolic site I pocket (amino acids A6 and A11 involved in the binding are depicted by a stick model); two initial orientations of serotonin, and dopamine were considered.

dynamic association with site III. Both methodologies excluded dopamine binding in site I. MD simulations also indicate preferential dopamine over serotonin binding to site III, whereas solid-state X-ray analyses yields only serotonin-site III complexes. In addition, crystal structures of serotonin-insulin hexamers loaded with arginine have been obtained that underline a possible more complex, physiological role of insulin-arginine interactions.

Results concerning site I complexes are corroborated by 4H3N spectroscopic experiments, which provide apparent binding constants for interaction of insulin hexamers with phenolic ligands and arginine. Our findings thus provide a novel insight into the storage mechanism of insulin in pancreatic β -cells, also relevant for novel insulin formulations for clinical applications.

Results

MD simulations of serotonin, dopamine, and phenol binding in site I

Here, we address the question of whether two neurotransmitters, serotonin and dopamine, can substitute phenol in its insulin R₆ hexamer binding site I. MD simulations were performed for the R₆ insulin hexamer, where site I-bound phenol was systematically replaced with neurotransmitters (each ligand in two steric-clash-free orientations; see Fig. 2). As expected, the MD simulations yielded the benchmark phenol-bound insulin R₆-state hexamer (InsPheR₆) with a low root mean square deviation (r.m.s.d.) of ~ 1.6 – 1.8 Å from the reference InsPheR₆ structure, indicating that the system does not

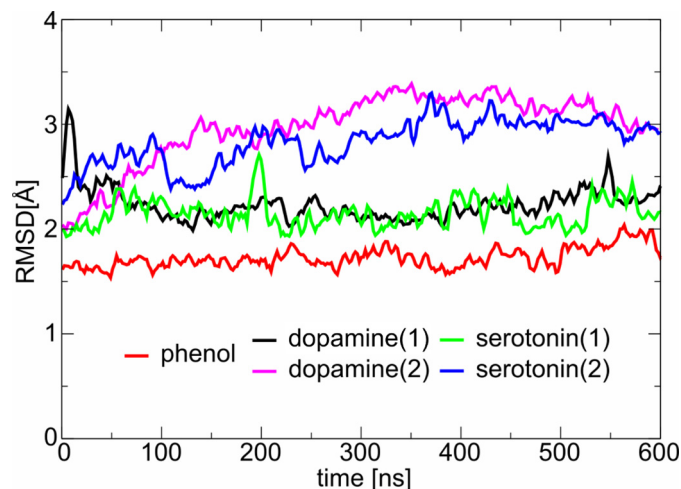


Figure 3. r.m.s.d. of the protein backbone (heavy atoms) from the insulin R₆ hexamer NMR structure with different phenolic ligands (phenol, dopamine, or serotonin). Labels 1 and 2 correspond to the two starting orientations of the neurotransmitter molecules.

deviate significantly from the NMR structure during the simulation (Fig. 3).

Both serotonin (InsSerR₆) and dopamine (InsDopR₆) complexes with ligands orientation (1) behaved similarly to InsPheR₆, with the backbone r.m.s.d. just above 2 Å. However, the starting orientation (2) of the ligands led to higher r.m.s.d. of ~ 2.8 Å (Fig. 2) indicating somewhat larger structural changes. A more direct insight into the behavior of the ligand in site I can be obtained from a direct comparison of their r.m.s.d. (Fig. 4).

The MD simulations confirm that phenol molecules are essentially fixed in site I with a minimal dynamic behavior. Two of the six phenols transiently break HBs (both with Cys^{A6} and Cys^{A11}); however, they remain in site I, eventually reestablishing the original geometry of binding. Similarly, all but one of the serotonin molecules in the starting conformation (1) stay in site I (only one serotonin ligand temporarily leaves this cavity). However, serotonin in starting geometry (2) as well as dopamine in both starting orientations, break most of the crucial hydrogen bonds. Serotonin, but not dopamine, thus essentially mimics phenol interactions observed in InsPheR₆ with its charged aminoethyl-group-forming HB with backbone carbonyl CO of Cys^{A11}, fitting well into the binding site I.

The strength of binding (*i.e.* the binding free energy and the corresponding dissociation constant) of phenol and the two neurotransmitters was calculated using the thermodynamic integration method (see Table 1). The free energy calculations confirmed and quantified the pattern observed in direct MD simulations, indicating a similarly strong binding of phenol and serotonin to site I (K_d of 5.4×10^{-4} M and 8.1×10^{-4} M, respectively) as well as demonstrating a lack of any stable conformation of dopamine in this cavity (reflected in a positive binding free energy).

MD simulations of serotonin and dopamine probing the hexamer surface sites

Initial simulations of the R₆ insulin hexamer with six dopamine molecules located in the phenolic pockets indicated that dopamine does not bind strongly to the phenolic pocket. At the

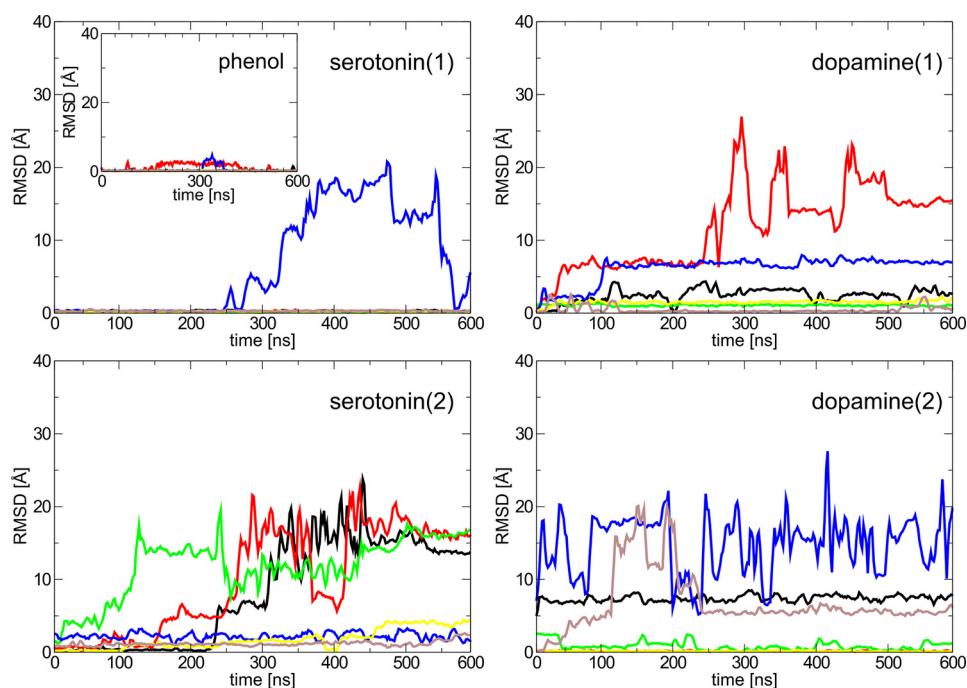


Figure 4. r.m.s.d. from simulations of all phenolic ligands (serotonin or dopamine in two orientations) from the phenol-binding pockets in the insulin R_6 hexamers (in total six phenolic ligands per one R_6 hexamer). Each line corresponds to the r.m.s.d. of one phenolic ligand from its starting position with respect to the O atom of Cys^{A6} and the N atom of Cys^{A11} involved in a hydrogen bond. A zero or small value of r.m.s.d. means a strong ligand, R_6 hexamer hydrogen bond, whereas a significant increase of r.m.s.d. indicates breaking of this bond.

Table 1

Standard free energies of binding of phenol, dopamine, and serotonin, molecules to the binding site I (phenolic pocket) together with the corresponding dissociation constants

Ligand	ΔG_b°	K_d
	<i>kcal/mol</i>	<i>[M]</i>
Phenol	-4.49 ± 1.55	5.4×10^{-4}
Dopamine	1.10 ± 1.73	6.3
Serotonin	-4.24 ± 1.87	8.1×10^{-4}

same time, several dopamine molecules left the phenolic pocket to bind to the hitherto unexplored site III at the surface of the insulin hexamer. Therefore, an additional set of calculations was performed to characterize the binding of neurotransmitters to the surface of the insulin R_6 hexamer (for simulation details, see the [supplemental information](#)). These simulations showed that dopamine binds at three equivalent binding sites in between the symmetry-related dimers (Fig. 5, *top*), which correspond to the previously sporadically observed site III. Analogous MD simulations for serotonin showed a similar mode of binding in site III but with a spatially looser neurotransmitter distribution, which reflects its weaker binding to this site compared with dopamine (Fig. 5, *bottom*). Finally, the binding of neurotransmitters at the surface sites has only a minor effect on the structure of the hexamer.

Both dopamine and serotonin bind in site III in a pocket between Glu^{A17} and Tyr^{A14} from neighboring dimers (Fig. 6). The stronger binding of dopamine over serotonin shown by free energy calculations (see below) results from its interactions with Tyr^{A14}, a hydrogen bond of the phenolic OH to Glu^{A17}, and a salt bridge between the aminoethyl group and the carboxylic group of Glu^{A17}. Similar interactions are present for serotonin; however, the steric fit is not as good as for dopamine.

Dopamine, serotonin, and phenol binding in site III were quantified by evaluation of the binding free energies and the corresponding dissociation constants (Fig. 7 and Table 2) using the umbrella sampling method, with symmetry and volume entropy corrections. In contrast to site I, dopamine is the strongest binder to site III (K_d 4.38×10^{-3} M), with serotonin and phenol showing a much weaker affinity for this surface site (K_d of 2.13×10^{-1} M and 2.59×10^{-1} M, respectively).

Insulin-serotonin crystal complex

The crystal structure of insulin grown in the presence of serotonin and Zn²⁺ revealed a T_3R_3 hexamer (referred to here as InsSer T_3R_3), with six neurotransmitters and two Zn²⁺ ions per hexamer (Fig. 8). The minimum serotonin concentration that still yielded complex crystals was within the 35–40 mM range. The asymmetric unit of this crystal contains 14 molecules of insulin, hence providing reliable, independent multi-copy structural evidence. The hexamer quaternary structure is indeed T_3R_3 as the B1–B3 N termini acquire here a more R-like (fully α -helical) fold rather than an R^f, “frayed,” conformation observed in $T_3R_3^f$ oligomers.

Coordination of both Zn²⁺ ions is tetrahedral regardless of the R or T protein environment with axial Cl[−] ligands. The overall fold of InsSer T_3R_3 is very similar to other $T_3R_3^f$ hexamers. For example, the r.m.s.d. of InsSer T_3R_3 from complexes with phenol (PDB ID 1MPJ Ref. 29), Tylenol (PDB ID 1TYL; Ref. 23), paraben (3 MTH; Ref. 29), and 4-hydroxy-benzamide (PDB ID 1BEN; Ref. 25) are 0.8911 Å, 0.9886 Å, 0.9105 Å, and 1.1570 Å, respectively. Also, this hexamer is not significantly different from phenol-free $T_3R_3^f$ hexamers induced by ions such as SCN[−] (PDB ID 2TCL, r.m.s.d. 0.9919 Å; Ref. 29) and Cl[−] (PDB ID 1G7A, r.m.s.d. 0.7765 Å (Ref. 38).

Structural forms of storage insulin in pancreas

Table 2

Standard free energies of binding of phenol, dopamine, and serotonin molecules to the binding site III and the corresponding dissociation constants

W_0 is free energy difference directly from umbrella sampling calculations, $\langle \Delta G_{\text{symm}} \rangle$ is hexamer symmetry contribution, ΔG_{vol} is volume entropy contribution (with respect to the standard state at 1 M), ΔG_b° is overall standard free energy of binding, and K_d is the corresponding dissociation constant.

Ligand in the binding site III	W_0	$\langle \Delta G_{\text{symm}} \rangle$	ΔG_{vol}	ΔG_b°	K_d
	<i>kcal/mol</i>	<i>kcal/mol</i>	<i>kcal/mol</i>	<i>kcal/mol</i>	<i>M</i>
Phenol	-1.83 ± 0.28	-0.36	1.38 ± 0.22	-0.81 ± 0.36	2.59×10^{-1}
Dopamine	-6.23 ± 0.67	-0.36	3.2 ± 0.2	-3.24 ± 0.70	4.38×10^{-3}
Serotonin	-2.65 ± 0.55	-0.36	2.0 ± 0.1	-0.92 ± 0.56	2.13×10^{-1}

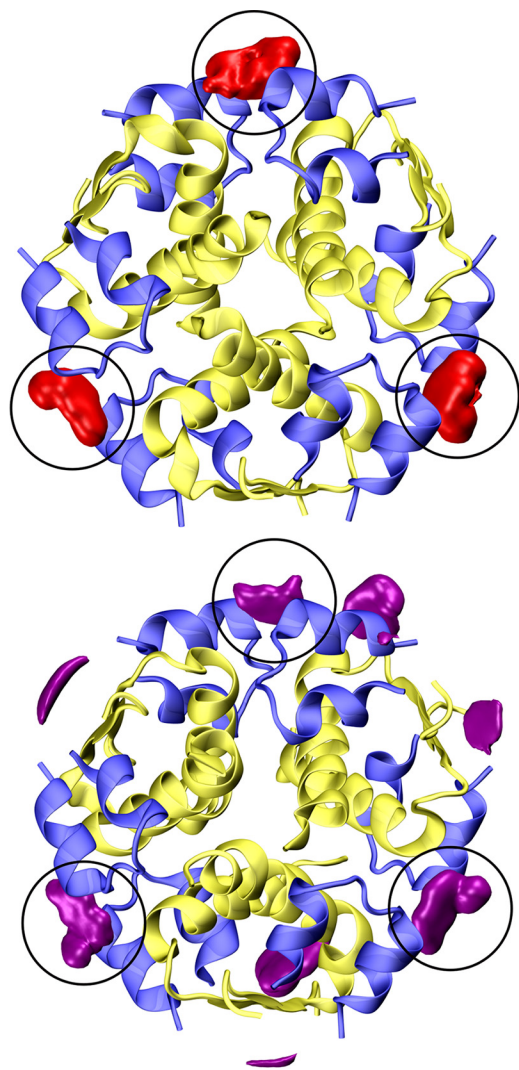


Figure 5. Dopamine (top, red) and serotonin (bottom, magenta) spatial distributions around the insulin R_6 hexamer (top view). The A/B-chains are in blue and yellow, respectively; the same isodensity value ($\sim 50\times$ the bulk concentration) was used for both neurotransmitters. Black circles depict the site III binding pockets.

Serotonin occupies six sites in InsSerT₃R₃: three phenol “main” sites I and three hexamer surface sites III. It is tethered (Fig. 9) into site I via (typical for phenolic ligands) HBs of its OH group to -CO of Cys^{A6} (range of 2.41–2.43 Å) and to -NH of Cys^{A11} (2.93–3.17 Å); a weaker HB -OH contact to -CO of Ser^{A9} (3.38–3.41 Å) further stabilizes this phenolic anchor. A significant His^{B5}-Nε2·π pyrrole HB (3.46–3.56 Å) contributes to the immobilization of the serotonin indole ring, which is assisted further by more subtle van der Waals (hydrophobic) interac-

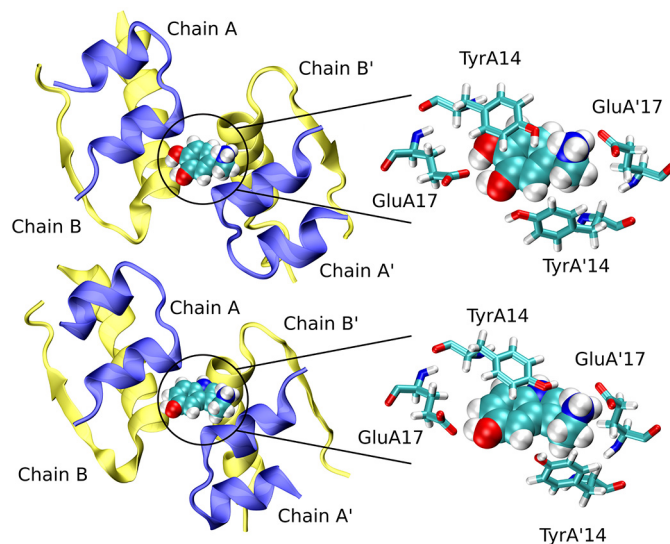


Figure 6. Serotonin (top) and dopamine (bottom) binding site III formed by two adjacent insulin monomers (Chain A/A' and Chain B/B'). Detailed structures of amino acids involved in binding (Glu^{A17} and Tyr^{A14}) are also shown.

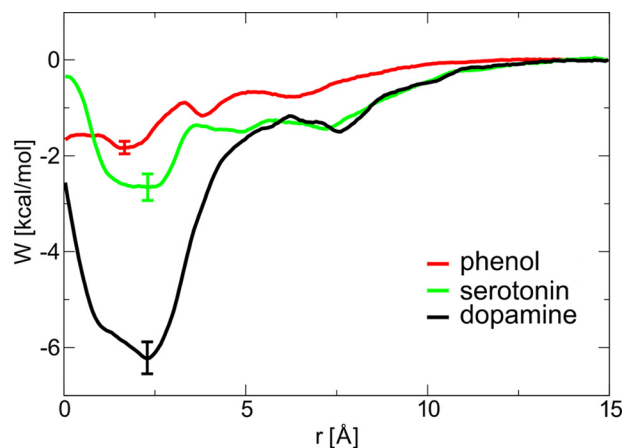


Figure 7. Free energy profiles of phenolic ligands entering the surface binding site III.

tions, especially with Leu^{B17} (3.45–3.59 Å). The aminoethyl side chain of serotonin points toward the surface of the hexamer, *i.e.* into the space/gap between two 3-fold related dimers. The -NζH amino group of this side chain is hydrogen-bonded to Oε1 of Glu^{B21} (2.55–2.75 Å) and -CO of Cys^{A11} (2.72–2.79 Å).

In contrast to site I, the serotonin-binding mode to site III is rather dynamic, indicating its mobility on the InsSerT₃R₃ surface. Although serotonin is pincer there in a hydrophobic clamp of Tyr^{A14} (π·π interactions ~ 3.5 Å) and the side chain of

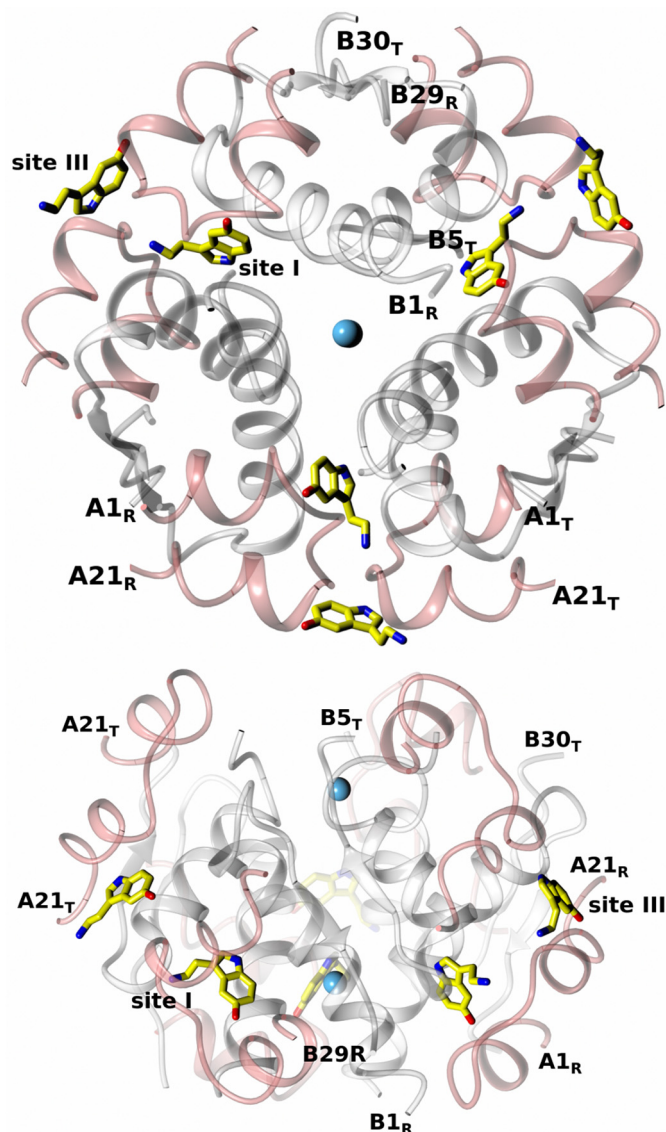


Figure 8. Serotonin binding sites in insulin $\text{InsSerT}_3\text{R}_3$ hexamer: top view (top), side view (bottom) of the hexamer (A-chains in pink, B-chains in white, Zn^{2+} ions as blue spheres). Sites I and III are indicated; some N and C termini of A/B-chains (T-state: T, R-state: R) are shown. Serotonin in atom-colored coded, with C-atoms in yellow.

Leu^{A13} (from a symmetry related dimer), the ligands' electron density is generally less well defined there. The serotonin phenolic OH group makes hydrogen bond to the O_ϵ atoms of Glu^{A17} (2.96–3.44 Å), and it can be stabilized by water-mediated HB to the hydroxyl of Tyr^{A14} . The HBs of the Glu^{A17} carboxylic side chain to the guanidinium group of Arg^{B22} (2.75–2.82 Å) contributes further to the structural stability of the serotonin-OH environment. However, it is evident that the aromatic moieties of Tyr^{A14} and serotonin can slide parallel to each other, indicating further adaptability of this mode of binding. Relative flexibility of site III is also seen in different modes of the HB network to the $-\text{N}\zeta$ group of the serotonin aminoethyl side chain. It is engaged primarily by HBs to the carboxyl side chain of Glu^{A17} (2.65–2.76 Å) and via a water molecule to Arg^{B22} , but this network of HBs is prone to disruption due to the flexibility of the serotonin surface-exposed side chain. In summary, the

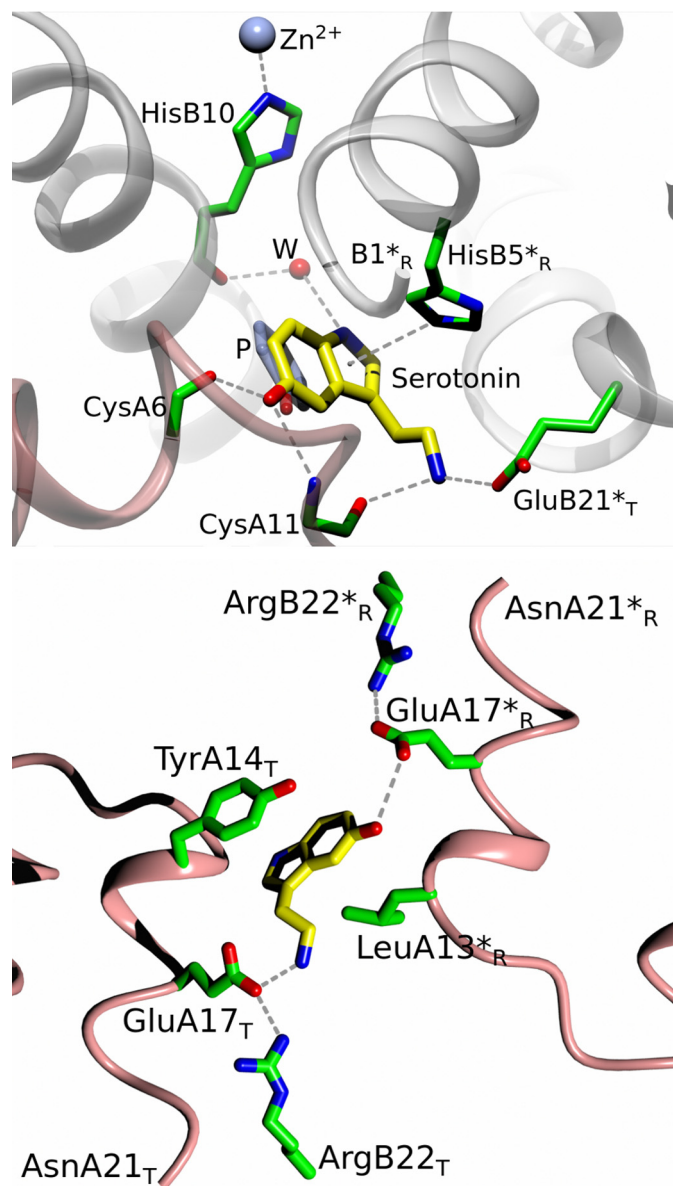


Figure 9. Serotonin binding sites: top, site I; bottom, site III, in insulin $\text{InsSerT}_3\text{R}_3$ complex (insulin color-coded as in Fig. 7, with side-chain C-atoms in green, water as a red sphere). Dashed lines, HB; *R and *T, correspond to symmetry-related dimer and T/R state of the monomer, respectively. Strong $\text{His}^{\text{B5}}-\text{N}\epsilon 2-\pi$ -pyrrole-center contact is also shown.

$\text{Glu}^{\text{A14}}/\text{Arg}^{\text{B22}}$ -pair are the 2-fold symmetry-related providers of HBs to serotonin (one pair to the ligand's OH group, the other one to the end of its side chain) in site III, but these HB networks are not fully symmetrical in overall geometry and strength due to a non-symmetrical ligand in this site. The swing of the other (not involved in serotonin binding) Tyr^{A14} side chain, away from site III, breaks down the 2-fold symmetry of this interface even further. Finally, we note that all our dopamine/insulin co-crystallizations were unsuccessful, likely due to the oxidation of the ligand, despite the inclusion of some anti-oxidation agents in the media.

Insulin-serotonin-arginine crystal complex

A similar set of crystallization conditions yielded crystals of insulin in a ternary complex with serotonin and arginine

Structural forms of storage insulin in pancreas

(referred to here as InsSerArgT₃R₃). Arginine- and Zn²⁺-containing crystallizations of insulin were carried out in the presence and absence of the previously established optimum serotonin concentration (40 mM). Serotonin-arginine-containing solutions yielded several morphologically different, but crystallographically very isomorphous, crystal forms. Despite their similarity, two of these forms (f1, f2) (referred to as InsSerArgf1-T₃R₃ and InsSerArgf2-T₃R₃) are reported here due to a dynamic (*i.e.* with high level of disorder) nature of Arg/insulin binding, hence the need for more independent structural evidence about the nature of these interactions.

Both InsSerArg complexes appear in the T₃R₃ hexamer state, with all Zn²⁺ ions in a tetrahedral coordination with Cl⁻ as an axial ion. They are very similar to the InsSerT₃R₃ complex, with overall r.m.s.d. values of 0.2193/0.2349 Å between these structures.

Despite the presence of arginine, the serotonin modes of binding in sites I are practically the same as in the Ins-Ser complex (Fig. 10). However, the site III shows more significant structural variety in binding of this neurotransmitter. Some serotonins in site III are bound in a fashion observed in InsSerT₃R₃; however, some of these ligands are flipped in both InsSerArgT₃R₃ crystal forms, *i.e.* the -OH and aminoethyl groups switch their positions. As both of them benefit from a similar HB network of symmetrical Glu^{A14}/Arg^{B22} tandems, the overall HB-connectivity is conserved here as well, with the exception of the Nζ atom of the aminoethyl side chain. It forms in some sites III a new HB with the hydroxyl group of Tyr^{A14} (2.67 Å) besides maintaining a HB to the side chain of Glu^{A14} as well.

It has to be stressed that several serotonins in site III and arginine molecules (see below) in the InsSerArgT₃R₃ complex have been refined with half-occupancies and, in some cases, with more arbitrary modeling due to their partial definition in the electron density maps. This reflects the dynamic and mobile character of some ligand/hormone interactions in InsSerArgT₃R₃ hexamers.

Arginine molecules occupy the “T-state-half” of the trimer (Fig. 11), with their Cα moieties being part of the T-state trimer surface (on the level with the Cl⁻ ion), whereas their side chains point toward the hexamer core, relatively parallel to its central axis. The aminocarboxy-Cα groups of Arg have been modeled in both InsSerArgT₃R₃ forms with some flipped/alternative conformations around the Cα atom.

The dominant stabilizations of the Arg Cα-end result from HBs of the carboxyl group to the NH of Cys^{B7} (2.76–3.31 Å) and amino acid amine group to CO of His^{B5} (2.86–3.18 Å). However, it is possible to model this part of arginine with alternative conformations, a likely effect of a dynamic character of these ligands at the wider, and more solvent-accessible, T₃ side of the hexamer.

In contrast, the HBs of the Arg guanidinium groups are much better defined, especially in the InsSerArgf2T₃R₃ form. One of their main signatures is the extensive HB network with both Glu^{B13} and His^{B10} residues. Here, the Glu^{B13} Oε1/Oε2 atom forms HBs to Arg Nη1 (2.11–2.33 Å) and Nδ1 of His^{B10} (2.82–3.14 Å), whereas the second Nη2 atom of the guanidinium group is hydrogen-bonded to CO of His^{B10} as well (2.71–2.82

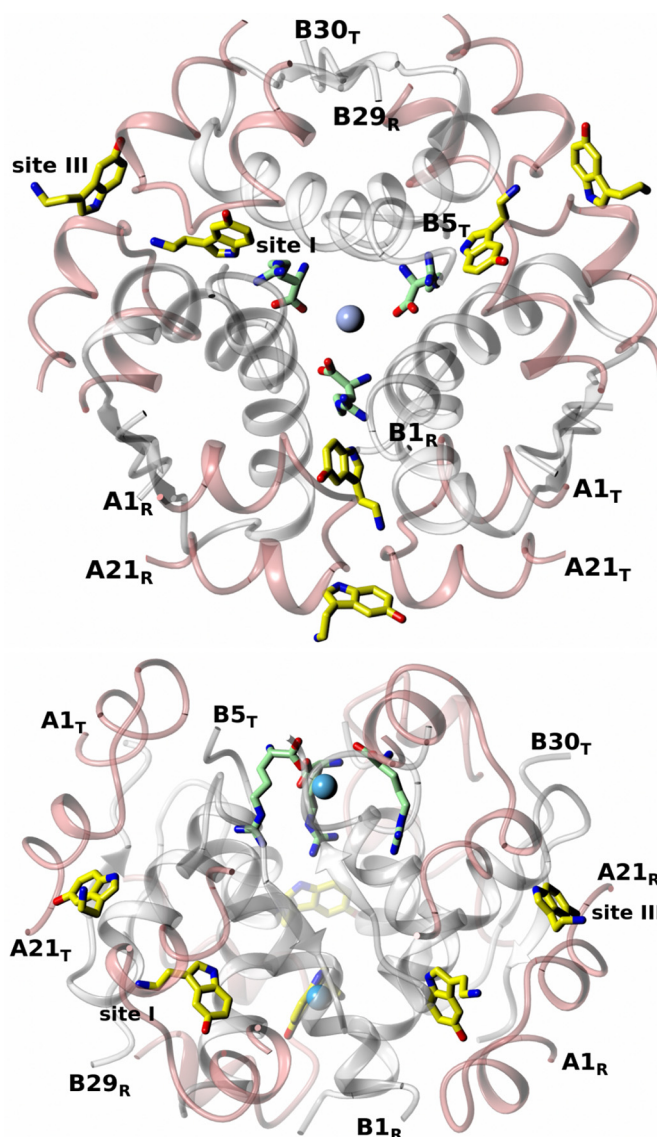


Figure 10. Serotonin and arginine binding sites in insulin InsSerArgT₃R₃ hexamer: top view (*top*) and side view (*bottom*) of the hexamer (labeling and color-coding as in Fig. 7, with arginine C-atoms in light green).

Å). The last guanidinium Ne1 atom locks this group by HB to the hydroxyl Oγ of Ser^{B9}. Some of these HBs are broken in the InsSerArgf1T₃R₃ form, also indicating the increased mobility of this environment, especially some shifting of the arginine parallel to the hexamer 3-fold axis.

Determination of ligand K_d values by solution 4H3N assay

The interactions of insulin hexamers with phenol, serotonin, dopamine, and arginine in solution were investigated and quantified by spectroscopic studies, with the 4H3N chromophore, which binds exclusively to His^{B10} sites in the R-state only, which is associated with the red shift of its absorption spectrum. This allows for the determination of the apparent binding constants (K_d) of selected ligands to insulin hexamers and estimation of the values of their maximum specific binding (B_{max}), which can be considered here as a measure of the amount of the R state induced by the ligand. In addition, the Hill coefficients (h), which indicate the scale of cooperativity (likely very com-

Structural forms of storage insulin in pancreas

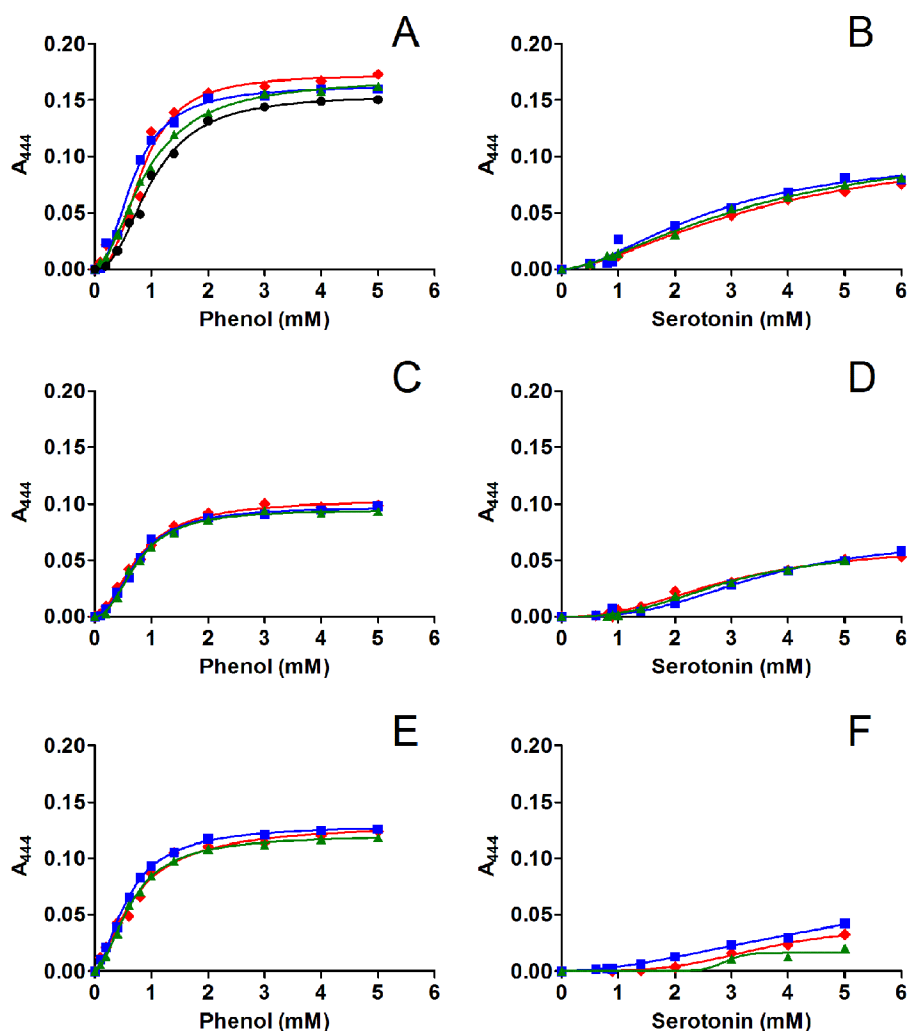


Figure 12. Titration of insulin hexamers and 4H3N with phenol (A) or serotonin (B). Titration of insulin hexamers and 4H3N preincubated with 5 mM arginine with phenol (C) or serotonin (D). Titration of insulin hexamers and 4H3N preincubated with 5 mM dopamine with phenol (E) or serotonin (F). All measured binding curves are shown.

Table 3

Values of K_d , B_{max} , and Hill coefficient (h) for the interaction of phenol or serotonin with insulin hexamers in the presence of 4H3N and/or arginine and serotonin

Ligand	$K_d \pm S.D.$	$B_{max} \pm S.D.$	$h \pm S.D.$
	<i>mm</i>		
Phenol ($n = 4$)	0.86 ± 0.13	0.17 ± 0.01	2.22 ± 0.30
Phenol and 5 mM Arg ($n = 3$)	0.75 ± 0.01	0.10 ± 0.00	2.07 ± 0.19
Phenol and 5 mM dopamine ($n = 3$)	0.64 ± 0.06	0.13 ± 0.01	1.68 ± 0.18
Serotonin ($n = 3$)	3.34 ± 0.52	0.11 ± 0.08	1.63 ± 0.10
Serotonin and 5 mM Arg ($n = 3$)	3.12 ± 0.31	0.06 ± 0.00	2.64 ± 0.27
Serotonin and 5 mM dopamine ($n = 3$)	3.93 ± 1.28	0.05 ± 0.04	7.12 ± 7.50

amine dispersion contribution to free energy of binding in the MD simulations is more negative compared with phenol. Rather, as the superposition of dopamine with phenol or serotonin ligands in site I suggests, the lack of dopamine binding is due to an electrostatic mismatch, namely its inability to accommodate the charged aminoethyl side chain in the site I cavity. The smaller aromatic scaffold of dopamine thus does not allow its side chain to reach the hexamer surface and form HBs observed in serotonin complexes.

As the 4H3N spectroscopic applicability was limited here to the environment of His^{B10} and, hence, the site I, the evidence for other insulin site-ligand interactions came solely from MD

simulations and X-ray crystallography. Both showed serotonin binding to surface site III, whereas only MD calculations predicted the possibility of a stable site III-dopamine complex (note, however, that dopamine-insulin co-crystallization may be hampered by a rapid chemical degradation/oxidation of dopamine). Interestingly, MD calculations indicated superior dopamine binding to site III, with its $K_d \sim 50$ times better than for phenol or serotonin. MD-predicted dopamine dominance at site III is interesting, as these simulations show its binding in a similar mode to serotonin-site III complex, which is observed both in MD simulations and crystal structures. Both neurotransmitters engage Tyr^{A14} and Glu^{A17}/Arg^{B22} side chains

from 2-fold symmetry-related dimers in the network of HB and π - π -stacking interactions. Moreover, crystal structures of InsSerT₃R₃ also underline the dynamical character of site III mode of binding, which involves flipping of the serotonin indole ring (*i.e.* swapping positions of -OH and the aminoethyl side chain) and a certain variability of the Tyr^{A14}-OH/Glu^{A17}/Arg^{B22} HB patterns.

The impact of these ligands, which are natural components of pancreatic β -cells insulin-storing LDCVs, was also extended from neurotransmitters to probing of arginine-insulin hexamer interactions. It was postulated earlier that arginine can accumulate in these granules upon processing of pro-insulin at its two sites (Arg-31–Arg-32 and Lys-64–Arg-65) (34, 35), which are cleaved by specific convertases during maturation of this hormone (42, 43). Here, the X-ray crystallography revealed that arginine can penetrate serotonin-containing hexamers (InsSerArgT₃R₃) without significant changes to their InsSerT₃R₃ state. Arginine is accommodated there in channels within the T₃ trimer, parallel to the hexamer 3-fold axis and opposite to R₃ trimer sites I filled by serotonin, which leads to filling the voids around Zn²⁺ and His-B10. Binding of arginine in InsSerArgT₃R₃ is dynamic with high mobility and alternative, slightly different ligand conformations. The flexibility of arginine is concentrated mostly around its -C α NH₂COO⁻ moieties, which form weak alternative HB to main chain groups of Cys^{B7} and His^{B5}, also exhibiting some flipping around the C α atom. In contrast, the guanidinium groups of the arginines are firmly engaged in extensive networks of HBs, which link them with side chains of Glu^{B13}, the side- and main-chain of His^{B10}, and the side chain of Ser^{B9}. This simultaneous binding of the two very different ligands to the T₃R₃ insulin hexamer polarizes this oligomer even further into two structurally distinct trimers, Arg₃T₃ and Ser₆R₃. Although Arg binding in the ArgT₃ trimer has a notable impact on the stability of the usually mobile Glu^{B13} side chains, the solvent-exposed flexible -C α NH₂COO⁻ moieties may contribute to the disorder of the N-terminal parts of B-helices, which is, however, untraceable up to the His^{B5} site in both arginine-containing and arginine-free serotonin complexes. In contrast, the Glu^{B13} side chains are fully disordered in the Ser₆R₃ trimer, whereas the serotonins in sites I facilitate fixing of the B1-B19 helices in the R-state.

The structural partition of Arg₃T₃ and Ser₆R₃ is more complex. First, although the site I pocket is mainly formed by two R-monomers, the T-state monomer also contributes here by Leu^{B17} and Glu^{B21} toward serotonin aromatic rings and side-chain binding, respectively. Secondly, serotonin surface site III also mediates the structural interface between T₃ and R₃, as this binding site (formed by Tyr^{A14}/Glu^{A17}) is provided by the T- and R-monomers from the 2-fold symmetry related dimers.

Interestingly, 4H3N spectroscopic data indicate that the presence of arginine increases (~13%) phenol (but not serotonin) affinity for site I and also increases the cooperative character of serotonin binding (as demonstrated by a higher Hill *h* factor). These structural and spectroscopic data provide evidence for the T₃-R₃ trimers cross-talk and, as postulated previously, for a heterotropic allostery within the insulin hexamer (22, 30, 44–47). However, the exact molecular detail behind this phenomenon has been elusive, likely involving a network of

propagating longer range interactions, which fit the Seydoux, Malhotra, and Bernhard (SMB) cooperativity model (48). The stabilizing effect of guanidinium groups on Glu^{B13}-His^{B10} and Zn²⁺ may be one of the initial steps in this process, priming the other half of the hexamer for more effective serotonin binding (*i.e.* an element of the so-called half-site reactivity). The stability of InsSerArgT₃R₃ and InsSerT₃R₃ hexamers in the presence of physiological ligands, *i.e.* trapping of these oligomers in a stable T₃R₃ state, agrees also with the finding that conformational fluctuations of the T₃ trimer needed for the appearance of site I become constrained upon formation of T₃R₃ (49). This can be considered as one of the features of the negative cooperativity effect in the insulin hexamer, predicted by the SMB model as well.

The present 4H3N spectroscopic data also suggest a dopamine-lowering effect of phenol's *K_d*. As there is no evidence for dopamine site I binding, this allosteric effect may result from longer-range cross-talk of the dopamine-site III complex with the environment of site I. On the other hand, dopamine does not seem to significantly change the serotonin *K_d*, and therefore, some “competitive” crowding effect (*e.g.* dynamic occlusion of site I) between these two neurotransmitters cannot be excluded. It may also mean that dopamine-site III binding facilitates the diffusion of a smaller ligand (*i.e.* phenol) into site I, whereas the increased stability of the insulin R₃-like trimer (via new HBs and interactions in site III) may obtrude its effect on binding of a larger ligand (such as serotonin).

It is worth mentioning that several tubular electron densities are also observed in InsSerArgT₃R₃ on the top of the T₃ trimer. These are linked with the modeled arginine ligands, suggesting the presence of more of these molecules on the hexamer surface, in the form of a hydrogen-binding network of ligands. Some of this electron density is in contact with the T₃ Zn²⁺ ion. Therefore, a contribution of the arginine -COO⁻ group to the tetrahedral/monodentate coordination of Zn²⁺ (observed also in the insulin R₆ structure; Ref. 41) cannot be excluded either. This direct arginine-Zn²⁺ interaction would hamper the T₃→R₃ transition even further, thus reinforcing the stability of the T₃R₃ hexamer.

Arginine is widely used *in vitro* as a nonspecific protein-folding stabilizing agent (49, 50), and so its presence in InsSerArgT₃R₃ structures may reflect some of its physiologically relevant roles as a ubiquitous insulin ligand. First, it may serve as an unspecific, granules-abundant, insulin-folding stabilizer and hexamer half-life enhancer. Second, it may act as a more specific endogenous ligand that modulates the hexamer cooperativity, also enhancing the stability of its particular T₃R₃ storage form. This more specific role of arginine may result, among others, from its guanidinium counterion-like neutralization of the repulsive system of the Glu^{B13} side chains in the hexamer core. Moreover, a simultaneous arginine-mediated cross-linking of Glu^{B13} side chains with Zn²⁺-binding His^{B10}, leading to stabilization of this structurally key region, further exemplifies the ligand-like role of this amino acid.

It has to be stressed that insulin crystallization in the granules can be also affected by the intragranular Zn²⁺ concentrations, which are modulated by some Zn²⁺ transporters (ZnT), especially by the disease-associated ZnT8 variants (51). However,

Structural forms of storage insulin in pancreas

the focus here was on insulin/neurotransmitter interactions, hence the experimental Zn^{2+} concentrations (0.4–8 mM) were maintained within typical insulin *in vitro* crystallization ranges. Interestingly, insulin crystallized here only in the form of 2Zn^{2+} hexamers, regardless the very high (25:1) Zn^{2+} -hormone molar excess in the crystal-yielding conditions.

There are ongoing efforts for a better insight into the size and content of insulin storage granules (e.g. Ref. 52). Their exocytosis can also be morphologically and mechanistically quite heterogeneous (so-called “kiss-and-run” phenomenon), releasing varying amounts and forms of granule content and on different time scales (53). Therefore, the final amount and form of insulin discharged to the circulation can be a very complex and multifactorial process; whether insulin-neurotransmitter-arginine hexamers are one of its variables remains to be seen.

Conclusions

We have demonstrated here that insulin oligomeric forms in storage granules in β -pancreatic cells could be regulated by certain endogenous components of these vesicles, such as serotonin, dopamine, and arginine. They are able to (i) shift the insulin oligomeric equilibrium toward the T_3R_3 state, which therefore may be considered as the insulin storage form in pancreatic β -cells, (ii) affect and modulate the allostery of the insulin hexamer, (iii) may provide folding stability and protection for the insulin hexamer, and consequently (iv), may have a direct role in the modulation of insulin release from β -cells *in vivo*. Moreover, these ligands can act in a synergistic, heterotropic fashion, pointing to a co-operative, complex, and dynamic nature of the interactions within the insulin hexamer.

Therefore, the importance of the neurotransmitters for insulin beta-cell biology can be either cumulative or even independent. Serotonin/dopamine are involved in the regulation of exocytosis of the granules, whereas their impact on insulin storage can be seen as a serendipitous side effect of the evolution of the hormone within the β -cell environment and its optimization for a particular, species-specific, physiological profile.

It is also tempting to consider serotonin/dopamine-human insulin interactions as molecular fingerprints of insulin evolution in the animal kingdom, as insulin-like hormones are expressed in neurons in many invertebrates (54). The newly discovered (and still puzzling) role of insulin in the central nervous system and the emergence of neurodegeneration-linked so-called type III diabetes thus places our findings in a much wider physiological context (55, 56).

In summary, we show here that the insulin hexamer can act as a macromolecular sponge, keen to bind and assimilate a variety of physiological ligands and ions. This suggests that clinical exploration and use of insulin-hexamer-stabilizing ligands, driven by steering of the pharmacokinetics of this hormone, may mirror its physiological canonical properties, rooted also in insulin evolution. Although the present work is aimed at shedding new light on the physiological storage state of this hormone, it may also open ways to novel approaches in medical formulations of insulin, toward its more desired closer to *in vivo* profile during subcutaneous injections administered in diabetes.

Experimental procedures

Molecular dynamics simulations

All MD simulations were performed using the AMBER 14 program (57, 58). In all simulations the AMBER ff03 protein force field (59) and SPC/E water model were used (60). Production simulations were performed in the isothermal-isobaric ensemble at ambient conditions of $T = 300$ K and $p = 1$ atm using the Berendsen barostat and thermostat (61). The only exception was thermodynamic integration calculations, where the temperature was controlled by a Langevin thermostat with a reference temperature of $T = 300$ K and a collision frequency of 5 ps^{-1} in order to avoid problems of non-ergodicity when the ligand is fully decoupled from its environment. 3D periodic boundary conditions were applied with a non-bonded interaction cutoff of 9 \AA . The long-range electrostatic interactions were accounted for using the particle mesh Ewald method (62) using a cubic spline interpolation. The density of the charge grid was $64 \times 64 \times 64$, and the direct sum threshold was 10^{-5} . Van der Waals interactions beyond the cutoff were treated using the continuum model correction for energy and pressure. All bonds containing hydrogen atoms were constrained using the SHAKE algorithm (63). A time step of 2 fs was employed.

Mildly acidic conditions (pH ~ 5.5) of insulin storage granules would generally tend to favor a fully protonated side chain of His^{B5} (64). However, due to zinc coordination the Ne2 atom of His^{B10} is actually deprotonated (65, 66). In addition, the six Glu^{B13} side chains in the middle region of the insulin hexamer were considered as deprotonated. The overall charge of the protein is, therefore, -6 . Initial simulations indicated diffusion of Na^+ cation/cations into the middle region. At least one Na^+ cation was always present in the middle region of the hexamer being placed to the middle region from the start of the simulation.

Substitution of the site I-bound phenol by the neurotransmitters serotonin or dopamine was also investigated. The R_6 -state insulin complex with six phenols in sites I (referred to here as InsPhe R_6) was used as a reference structure (PDB ID 1AIY) due to a higher stability of this conformer and homogeneous saturation of insulin hexamer with the same ligand (67). The starting structures for simulations were obtained by exchanging phenol molecules in site I by either dopamine or serotonin molecules with two initial conformations for each ligand. The ligands were built from the phenol core (1 oxygen atom and 6 carbon atoms), the structure of which was available from X-ray structure). Subsequent restrained minimization eliminated any potential steric clashes. Starting geometries of phenolic ligands inside the phenolic pockets are depicted in Fig. 2.

Phenol, serotonin, and dopamine were assigned parameters from ff03 AMBER force field using the ANTECHAMBER package (68). Both serotonin and dopamine have a charge of $+1 e$ at pH 5.5. Partial atomic charges were obtained by the RESP (Restrained Electrostatic Potential Fit) (83) method, calculated at the HF/6-31G+ level, and they are listed in [supplemental Table S2](#), with the explanation in the [supplemental Figure S5](#). These calculations were performed using the Gaussian 09 package (69).

The B10-Zn interaction potential had to be re-parametrized in order to account (at least partially) for the electronic polarization and charge transfer effects and thus to reproduce experimental data. The charges on zinc ions and on His^{B10} were modified according to the results from *ab initio* calculations on small model systems to +1.5 *e* and +0.1677 *e*, respectively. These were obtained using the RESP/NPA (Natural Population Analysis) (84) analysis employing the B3LYP/aug-cc-pvtz level of theory (85, 86). In a similar spirit, to account for electronic polarization effects in a mean-field way (70–73), we rescaled bulk Na⁺ and Cl[−] (including the Na⁺ cation located in the middle of the hexamer) ionic charges by a factor of 0.75.

Each of the liganded insulin R₆ hexamers was immersed into a unit cell containing 9000 SPC/E water molecules, with Na⁺/Cl[−] ions added to acquire overall electroneutrality with no excess of salt present. After preparation, the energy of each of the systems was minimized using 5000 steps of the steepest descent method, where the protein and phenolic ligands were restrained with a harmonic potential. The systems were then subjected to 200 ps of isothermal-isochoric molecular dynamics, where the temperature was slowly raised from 10 to 300 K. This was followed by 1.2 ns of an isothermal-isobaric equilibration, which led to an equilibrated cell size of ~69 × 68 × 66 Å³. Systems were assessed as equilibrated by monitoring temperature, cell size, density, and root mean square displacement of the protein. After equilibration, the production runs were propagated for 600 ns.

In addition to direct MD simulations free energy calculations employing the thermodynamic integration method were performed to determine apparent binding constants *K_d* of phenol and the two neurotransmitters to the R₆ hexamer. The free energy cycles and further details of these simulations are presented in the [supplemental Figs. S6 and S7, and Table S3](#). Similar free energy calculations for evaluation of the *K_d* values to ligand binding sites III were performed using the umbrella sampling methods (for more details see the [supplemental information, and Table S4](#)). Here, to stabilize the hexamer R₆ state, site I was filled with phenol before the search for dopamine site III binding mode, as this neurotransmitter did not bind to site I in MD simulations.

X-ray crystallography

Crystallizations of all insulin complexes reported here were performed with the in-house insulin crystallization screens that cover most of the previously reported crystal growth parameters. Crystallization conditions, data collection, refinement, and models statistics as well as PDB codes are provided in [supplemental Table S1](#). All crystals were directly flash-cooled in liquid N₂. X-ray data were collected at 100 K and processed by *xia2* (74), and model building and refinement (*F* > 0σ*F*) were performed by COOT (75) and the CCP4 suite of programs (76). Crystal structures were solved by Molrep (77) with the B1-B6-truncated insulin hexamer, hexamer-derived dimer, and insulin monomer as a model (based on PDB ID 1MSO; Ref. 78) and refined by Refmac 5.8 (79). Examples of electron density maps are shown in [supplemental Figs. S3 and S4](#). The figures were made using CCP4mg (80). For structural comparisons, all insulin hexamer structures were superimposed in COOT by the

SSM fit option. For comparison of the site I ligand-binding modes, the relevant dimers were superimposed by Cα matching of the B9–19 helix for one of the monomers by the LSQ option in COOT.

Determination of ligand *K_d* values by a solution 4H3N assay

Solution studies of the interactions of phenol, serotonin, dopamine, and arginine with porcine insulin were performed following the protocols by Huang *et al.* (81), Bloom *et al.* (82), and Huus *et al.* (46). An anionic ligand 4H3N was used as a sensitive chromophoric probe to determine ligand binding curves by monitoring UV-visible absorption. 4H3N binds only in the insulin R-state (in the vicinity of His^{B10}), which red-shifts its absorption spectrum. The samples were dissolved in 10 mM potassium phosphate buffer at pH 7.4. In all measurements porcine hexameric Zn²⁺-insulin (two atoms of zinc per one hexamer) and 4H3N were used at 0.6 mM and 0.225 mM concentrations, respectively. Insulin was preincubated with 4H3N in a total volume 0.6 ml for 20 min at room temperature, after which a particular ligand (phenol, serotonin, dopamine, or arginine) was added in a minimum volume (0.6–3 μl) of 10 mM potassium phosphate buffer. After 15 min of reverse transcription equilibration, the UV-visible absorbance spectra were collected on a Perkin, Lambda 25 UV-visible Spectrometer. The spectra were taken in the range of 300–550 nm, and the difference spectra at λ_{max} of 444 nm were obtained by subtracting the absorbance of ligand-free 4H3N from the absorbance of ligand-bound 4H3N. The binding curves were analyzed using a method of non-linear regression and a fitting program considering one-site specific binding with a Hill slope using GraphPad Prism 5.0. The final *K_d*, B_{max}, and *h* values with standard errors were calculated from at least three independently determined binding curves for each system.

Author contributions—V. P. carried out the MD simulations. C. M. V., M. K., and T. R. G. carried out the crystallographic experiments. K. K. and P. H. carried out the solution 4H3N assays. J. P. T. collected the crystallographic data. A. M. B., P. J., J. J., and L. Z. conceived the study, designed the experiments, and analyzed the data. A. M. B., P. J., and J. J. wrote the paper. All authors discussed the results and commented on the manuscript.

Acknowledgments—We thank Diamond Light Source for access to their beam lines (proposal numbers mx-7864 and mx-9948), which contributed to the results presented here. We thank Sam Hart for assistance with data collection and Hayley Arthurs for crystallizations.

References

1. Taniguchi, C. M., Emanuelli, B., and Kahn, C. R. (2006) Critical nodes in signalling pathways: insights into insulin action. *Nat. Rev. Mol. Cell Biol.* **7**, 85–96
2. Cohen, P. (2006) Timeline: the twentieth century struggle to decipher insulin signalling. *Nat. Rev. Mol. Cell Biol.* **7**, 867–873
3. Atkinson, M. A., Eisenbarth, G. S., and Michels, A. W. (2014) Type 1 diabetes. *Lancet* **383**, 69–82
4. Taylor, S. I., Accili, D., and Imai, Y. (1994) Insulin resistance or insulin deficiency: which is the primary cause of Niddm. *Diabetes* **43**, 735–740
5. Turner, R. C., Hattersley, A. T., Shaw, J. T., and Levy, J. C. (1995) Type-II Diabetes: clinical aspects of molecular biological studies. *Diabetes* **44**, 1–10

Structural forms of storage insulin in pancreas

- Giovannucci, E., Harlan, D. M., Archer, M. C., Bergenstal, R. M., Gapstur, S. M., Habel, L. A., Pollak, M., Regensteiner, J. G., and Yee, D. (2010) Diabetes and cancer: a consensus report. *CA Cancer J. Clin.* **60**, 207–221
- Vigneri, P., Frasca, F., Sciacca, L., Pandini, G., and Vigneri, R. (2009) Diabetes and cancer. *Endocr. Relat. Cancer* **16**, 1103–1123
- Cohen, D. H., and LeRoith, D. (2012) Obesity, type 2 diabetes, and cancer: the insulin and IGF connection. *Endocr. Relat. Cancer* **19**, F27–F45
- Arrieta-Cruz, I., and Gutiérrez-Juárez, R. (2016) The role of insulin resistance and glucose metabolism dysregulation in the development of Alzheimer's disease. *Rev. Invest. Clin.* **68**, 53–58
- McKern, N. M., Lawrence, M. C., Streltsov, V. A., Lou, M. Z., Adams, T. E., Lovrecz, G. O., Elleman, T. C., Richards, K. M., Bentley, J. D., Pilling, P. A., Hoyne, P. A., Cartledge, K. A., Pham, T. M., Lewis, J. L., Sankovich, S. E., et al. (2006) Structure of the insulin receptor ectodomain reveals a folded-over conformation. *Nature* **443**, 218–221
- Lemmon, M. A., and Schlessinger, J. (2010) Cell signaling by receptor tyrosine kinases. *Cell* **141**, 1117–1134
- Adams, N. M. J., Blundell, T. L., Dodson, E. J., Dodson, G. G., Vijayan, M., Baker, E. N., Harding, M. M., Hodgkin, D. C., Rimmer, B., and Sheat, S. (1969) Structure of rhombohedral 2 zinc insulin crystals. *Nature* **224**, 491–495
- Dodson, G., and Steiner, D. (1998) The role of assembly in insulin's biosynthesis. *Curr. Opin. Struct. Biol.* **8**, 189–194
- Mayer, J. P., Zhang, F., and DiMarchi, R. D. (2007) Insulin structure and function. *Biopolymers* **88**, 687–713
- Ward, C. W., and Lawrence, M. C. (2011) Landmarks in insulin research. *Front. Endocrinol.* **2**, 76
- Weiss, M. A. (2009) The structure and function of insulin: decoding the TR transition. In *Insulin and IGFs* (Litwack, G., ed.), pp. 33–49, Elsevier Academic Press, Inc., San Diego CA
- Menting, J. G., Whittaker, J., Margetts, M. B., Whittaker, L. J., Kong, G. K., Smith, B. J., Watson, C. J., Záková, L., Kletvíková, E., Jiráček, J., Chan, S. J., Steiner, D. F., Dodson, G. G., Brzozowski, A. M., Weiss, M. A., Ward, C. W., and Lawrence, M. C. (2013) How insulin engages its primary binding site on the insulin receptor. *Nature* **493**, 241–245
- Menting, J. G., Yang, Y., Chan, S. J., Phillips, N. B., Smith, B. J., Whittaker, J., Wickramasinghe, N. P., Whittaker, L. J., Pandeyarajan, V., Wan, Z. L., Yadav, S. P., Carroll, J. M., Stokes, N., Roberts, C. T., Jr., Ismail-Beigi, F., et al. (2014) Protective hinge in insulin opens to enable its receptor engagement. *Proc. Natl. Acad. Sci. U.S.A.* **111**, E3395–E3404
- Derewenda, U., Derewenda, Z., Dodson, E. J., Dodson, G. G., Reynolds, C. D., Smith, G. D., Sparks, C., and Swenson, D. (1989) Phenol stabilizes more helix in a new symmetrical zinc insulin hexamer. *Nature* **338**, 594–596
- Bentley, G., Dodson, E., Dodson, G., Hodgkin, D., and Mercola, D. (1976) Structure of insulin in 4-zinc insulin. *Nature* **261**, 166–168
- Smith, G. D., Swenson, D. C., Dodson, E. J., Dodson, G. G., and Reynolds, C. D. (1984) Structural stability in the 4-zinc human insulin hexamer. *Proc. Natl. Acad. Sci. U.S.A.* **81**, 7093–7097
- Brzović, P. S., Choi, W. E., Borchardt, D., Kaarsholm, N. C., and Dunn, M. F. (1994) Structural asymmetry and half-site reactivity in the T to R allosteric transition of the insulin hexamer. *Biochemistry* **33**, 13057–13069
- Smith, G. D., and Ciszak, E. (1994) The structure of a complex of hexameric insulin and 4'-hydroxyacetanilide. *Proc. Natl. Acad. Sci. U.S.A.* **91**, 8851–8855
- Whittingham, J. L., Chaudhuri, S., Dodson, E. J., Moody, P. C., and Dodson, G. G. (1995) X-ray crystallographic studies on hexameric insulins in the presence of helix-stabilizing agents, thiocyanate, methylparaben, and phenol. *Biochemistry* **34**, 15553–15563
- Smith, G. D., Ciszak, E., and Pangborn, W. (1996) A novel complex of a phenolic derivative with insulin: structural features related to the T→R transition. *Protein Sci.* **5**, 1502–1511
- Dunn, M. F. (2005) Zinc-ligand interactions modulate assembly and stability of the insulin hexamer: a review. *Biometals* **18**, 295–303
- Ciszak, E., and Smith, G. D. (1994) Crystallographic evidence for dual coordination around zinc in the T3R3 human insulin hexamer. *Biochemistry* **33**, 1512–1517
- Smith, G. D. (1998) The phenolic binding site in T3R3f insulin. *J. Mol. Struct.* **470**, 71–80
- Whittingham, J. L., Edwards, D. J., Antson, A. A., Clarkson, J. M., and Dodson, G. G. (1998) Interactions of phenol and m-cresol in the insulin hexamer, and their effect on the association properties of B28 Pro → Asp insulin analogues. *Biochemistry* **37**, 11516–11523
- Rahuel-Clermont, S., French, C. A., Kaarsholm, N. C., Dunn, M. F., and Chou, C. I. (1997) Mechanisms of stabilization of the insulin hexamer through allosteric ligand interactions. *Biochemistry* **36**, 5837–5845
- Falck, B., and Hellman, B. (1963) Evidence for presence of biogenic amines in pancreatic islets. *Experientia* **19**, 139–140
- Lundquist, I., Ekholm, R., and Ericson, L. E. (1971) Monoamines in pancreatic-islets of mouse 5-hydroxytryptamine as an intracellular modifier of insulin secretion and hypoglycemic action of monoamine-oxidase inhibitors. *Diabetologia* **7**, 414–422
- Ustione, A., Piston, D. W., and Harris, P. E. (2013) Minireview: dopaminergic regulation of insulin secretion from the pancreatic islet. *Mol. Endocrinol.* **27**, 1198–1207
- Julius, D., Brake, A., Blair, L., Kunisawa, R., and Thorner, J. (1984) Isolation of the putative structural gene for the lysine-arginine-cleaving endopeptidase required for processing of yeast prepro-alpha-factor. *Cell* **37**, 1075–1089
- Fricker, L. D., Evans, C. J., Esch, F. S., and Herbert, E. (1986) Cloning and sequence analysis of cDNA for bovine carboxypeptidase-E. *Nature* **323**, 461–464
- Hagedorn, H. C., Jensen, B. N., Krarup, N. B., and Wodstrup, I. (1936) Protamine insulin. *JAMA* **106**, 177–180
- Norrman, M., Hubálek, F., and Schluckebier, G. (2007) Structural characterization of insulin NPH formulations. *Eur. J. Pharm. Sci.* **30**, 414–423
- Smith, G. D., Pangborn, W. A., and Blessing, R. H. (2001) Phase changes in T3R3f human insulin: temperature or pressure induced? *Acta Crystallogr. D* **57**, 1091–1100
- Bentley, G., Dodson, G., and Lewitova, A. (1978) Rhombohedral insulin crystal transformation. *J. Mol. Biol.* **126**, 871–875
- Wagner, A., Diez, J., Schulze-Briese, C., and Schluckebier, G. (2009) Crystal structure of ultralente: a microcrystalline insulin suspension. *Proteins* **74**, 1018–1027
- Steengaard, D. B., Schluckebier, G., Strauss, H. M., Norrman, M., Thomsen, J. K., Friderichsen, A. V., Havelund, S., and Jonassen, I. (2013) Ligand-controlled assembly of hexamers, dihexamers, and linear multihexamer structures by the engineered acylated insulin degludec. *Biochemistry* **52**, 295–309
- Smeekens, S. P., Avruch, A. S., LaMendola, J., Chan, S. J., and Steiner, D. F. (1991) Identification of a cDNA encoding a 2nd putative prohormone convertase related to Pc2 in AtT20 cells and islets of Langerhans. *Proc. Natl. Acad. Sci. U.S.A.* **88**, 340–344
- Smeekens, S. P., and Steiner, D. F. (1990) Identification of a human insulinoma cDNA encoding a novel mammalian protein structurally related to the yeast dibasic processing protease Kex2. *J. Biol. Chem.* **265**, 2997–3000
- Brader, M. L., Kaarsholm, N. C., Lee, R. W., and Dunn, M. F. (1991) Characterization of the R-state insulin hexamer and its derivatives: the hexamer is stabilized by heterotropic ligand-binding interactions. *Biochemistry* **30**, 6636–6645
- Choi, W. E., Brader, M. L., Aguilar, V., Kaarsholm, N. C., and Dunn, M. F. (1993) The allosteric transition of the insulin hexamer is modulated by homotropic and heterotropic interactions. *Biochemistry* **32**, 11638–11645
- Huus, K., Havelund, S., Olsen, H. B., Sigurskjold, B. W., van de Weert, M., and Frokjaer, S. (2006) Ligand binding and thermostability of different allosteric states of the insulin zinc-hexamer. *Biochemistry* **45**, 4014–4024
- Lisi, G. P., Png, C. Y., and Wilcox, D. E. (2014) Thermodynamic contributions to the stability of the insulin hexamer. *Biochemistry* **53**, 3576–3584
- Seydoux, J., and Girardie, L. (1974) Evidence for 2 receptor areas in brown adipose-tissue (Bat). *Experientia* **30**, 683–683
- Arakawa, T., Ejima, D., Tsumoto, K., Obeyama, N., Tanaka, Y., Kita, Y., and Timasheff, S. N. (2007) Suppression of protein interactions by arginine: a proposed mechanism of the arginine effects. *Biophys. Chem.* **127**, 1–8

50. Nuhu, M. M., and Curtis, R. (2015) Arginine dipeptides affect insulin aggregation in a pH- and ionic strength-dependent manner. *Biotechnol. J.* **10**, 404–416
51. Nicolson, T. J., Bellomo, E. A., Wijesekara, N., Loder, M. K., Baldwin, J. M., Gyulkhandanyan, A. V., Koshkin, V., Tarasov, A. I., Carzaniga, R., Kronenberger, K., Taneja, T. K., da Silva Xavier, G., Libert, S., Froguel, P., Scharfmann, R., *et al.* (2009) Insulin storage and glucose homeostasis in mice null for the granule zinc transporter ZnT8 and studies of the type 2 diabetes-associated variants. *Diabetes* **58**, 2070–2083
52. Fava, E., Dehghany, J., Ouwendijk, J., Müller, A., Niederlein, A., Verkade, P., Meyer-Hermann, M., and Solimena, M. (2012) Novel standards in the measurement of rat insulin granules combining electron microscopy, high-content image analysis and in silico modelling. *Diabetologia* **55**, 1013–1023
53. Tsuboi, T., and Rutter, G. A. (2003) Multiple forms of “kiss-and-run” exocytosis revealed by evanescent wave microscopy. *Curr. Biol.* **13**, 563–567
54. Conlon, J. M. (2001) Evolution of the insulin molecule: insights into structure activity and phylogenetic relationships. *Peptides* **22**, 1183–1193
55. Chami, B., Steel, A. J., De La Monte, S. M., and Sutherland, G. T. (2016) The rise and fall of insulin signaling in Alzheimer’s disease. *Metab. Brain. Dis.* **31**, 497–515
56. Steen, E., Terry, B. M., Rivera, E. J., Cannon, J. L., Neely, T. R., Tavares, R., Xu, X. J., Wands, J. R., and de la Monte, S. M. (2005) Impaired insulin and insulin-like growth factor expression and signaling mechanisms in Alzheimer’s disease: is this type 3 diabetes? *J. Alzheimers Dis.* **7**, 63–80
57. Case, D. A., Babin, V., Berryman, J. T., Betz, R. M., Cai, Q., Cerutti, D. S., Cheatham, T. E., Darden, T. A., Duke, R. E., Gohlke, A. W., Goetz, A. W., Gusarov, S., Homeyer, N., Janowski, P., Kaus, J., *et al.* (2014) *AMBER 14*, University of California, San Francisco
58. Salomon-Ferrer, R., Götz, A. W., Poole, D., Le Grand, S., and Walker, R. C. (2013) Routine microsecond molecular dynamics simulations with AMBER on GPUs. 2. Explicit solvent particle mesh Ewald. *J. Chem. Theory Comput.* **9**, 3878–3888
59. Duan, Y., Wu, C., Chowdhury, S., Lee, M. C., Xiong, G., Zhang, W., Yang, R., Cieplak, P., Luo, R., Lee, T., Caldwell, J., Wang, J., and Kollman, P. (2003) A point-charge force field for molecular mechanics simulations of proteins based on condensed-phase quantum mechanical calculations. *J. Comput. Chem.* **24**, 1999–2012
60. Berendsen, H. J. C., Grigera, J. R., and Straatsma, T. P. (1987) The missing term in effective pair potentials. *J. Phys. Chem.* **91**, 6269–6271
61. Berendsen, H. J. C., Postma, J. P. M., Vangunsteren, W. F., Dinola, A., and Haak, J. R. (1984) Molecular dynamics with coupling to an external bath. *J. Chem. Phys.* **81**, 3684–3690
62. Essmann, U., Perera, L., Berkowitz, M. L., Darden, T., Lee, H., and Pedersen, L. G. (1995) A smooth particle mesh Ewald method. *J. Chem. Phys.* **103**, 8577–8593
63. Miyamoto, S., and Kollman, P. A. (1992) Settle: an analytical version of the shake and rattle algorithm for rigid water models. *J. Comput. Chem.* **13**, 952–962
64. Hutton, J. C. (1982) The internal pH and membrane potential of the insulin-secretory granule. *Biochem. J.* **204**, 171–178
65. Ishikawa, T., Chatake, T., Morimoto, Y., Maeda, M., Kurihara, K., Tanaka, I., and Niimura, N. (2008) An abnormal pK (a) value of internal histidine of the insulin molecule revealed by neutron crystallographic analysis. *Biochem. Biophys. Res. Commun.* **376**, 32–35
66. Bryant, C., Spencer, D. B., Miller, A., Bakaysa, D. L., McCune, K. S., Maple, S. R., Pekar, A. H., and Brems, D. N. (1993) Acid stabilization of insulin. *Biochemistry* **32**, 8075–8082
67. Chang, X., Jorgensen, A. M., Bardrum, P., and Led, J. J. (1997) Solution structures of the R-6 human insulin hexamer. *Biochemistry* **36**, 9409–9422
68. Wang, J., Wang, W., Kollman, P. A., and Case, D. A. (2006) Automatic atom type and bond type perception in molecular mechanical calculations. *J. Mol. Graph. Model* **25**, 247–260
69. Frisch, M. J. T., Schlegel, G. W. H. B., Scuseria, G. E., Robb, M. A., Cheeseman, J. R., Scalmani, G., Barone, V., Mennucci, B., Petersson, G. A., Nakatsuji, H., Caricato, M., Li, X., Hratchian, *et al.* (2009) Gaussian 09, Revision A.1. Wallingford, CT
70. Leontyev, I., and Stuchebrukhov, A. (2011) Accounting for electronic polarization in non-polarizable force fields. *Phys. Chem. Chem. Phys.* **13**, 2613–2626
71. Leontyev, I. V., and Stuchebrukhov, A. A. (2012) Polarizable mean-field model of water for biological simulations with AMBER and CHARMM force fields. *J. Chem. Theory Comput.* **8**, 3207–3216
72. Leontyev, I. V., and Stuchebrukhov, A. A. (2014) Polarizable molecular interactions in condensed phase and their equivalent nonpolarizable models. *J. Chem. Phys.* **141**, 014103
73. Kohagen, M., Mason, P. E., and Jungwirth, P. (2016) Accounting for electronic polarization effects in aqueous sodium chloride via molecular dynamics aided by neutron scattering. *J. Phys. Chem. B* **120**, 1454–1460
74. Winter, G. (2010) xia2: an expert system for macromolecular crystallography data reduction. *J. Appl. Crystallogr.* **43**, 186–190
75. Emsley, P., and Cowtan, K. (2004) Coot: model-building tools for molecular graphics. *Acta Crystallogr. D* **60**, 2126–2132
76. Collaborative Computational Project, Number 4 (1994) The Ccp4 suite: programs for protein crystallography. *Acta Crystallogr. D* **50**, 760–763
77. Vagin, A., and Teplyakov, A. (1997) MOLREP: an automated program for molecular replacement. *J. Appl. Crystallogr.* **30**, 1022–1025
78. Smith, G. D., Pangborn, W. A., and Blessing, R. H. (2003) The structure of T-6 human insulin at 1.0 angstrom resolution. *Acta Crystallogr. D Biol. Crystallogr.* **59**, 474–482
79. Murshudov, G. N., Vagin, A. A., and Dodson, E. J. (1997) Refinement of macromolecular structures by the maximum-likelihood method. *Acta Crystallogr. D* **53**, 240–255
80. McNicholas, S., Potterton, E., Wilson, K. S., and Noble, M. E. (2011) Presenting your structures: the CCP4mg molecular-graphics software. *Acta Crystallogr. D* **67**, 386–394
81. Huang, S. T., Choi, W. E., Bloom, C., Leuenberger, M., and Dunn, M. F. (1997) Carboxylate ions are strong allosteric ligands for the His^{B10} sites of the R-state insulin hexamer. *Biochemistry* **36**, 9878–9888
82. Bloom, C. R., Wu, N., Dunn, A., Kaarsholm, N. C., and Dunn, M. F. (1998) Comparison of the allosteric properties of the Co(II)- and Zn(II)-substituted insulin hexamers. *Biochemistry* **37**, 10937–10944
83. Cornell, W. D., Cieplak, P., Bayly, C. I., and Kollman, P. A. (1993) Application of RESP charges to calculate conformational energies, hydrogen bond energies, and free energies of solvation. *J. Am. Chem. Soc.* **115**, 9620–9631
84. Reed, A. E., Weinstock, R. B., and Weinhold F. (1985) Natural population analysis. *J. Chem. Phys.* **83**, 735–746
85. Becke, A. D. (1993) Density-functional thermochemistry. III. The role of exact exchange. *J. Chem. Phys.* **98**, 5648–5652
86. Lee, C., Yang, W., and Parr, R. G. (1988) Development of the Colle-Salvetti correlation-energy formula into a functional of the electron density. *Phys. Rev. B* **37**, 785–789